J. Fluid Mech. (1970), *vol.* 40, *part* 1, *pp.* 161–189
Printed in Great Britain

The flat plate trailing edge problem

By FRANK E. TALKE† AND STANLEY A. BERGER
University of California at Berkeley

(Received 24 February 1969 and in revised form 24 June 1969)

The trailing edge region of a finite flat plate in laminar, incompressible flow is examined for the limit of high Reynolds numbers.

It is shown that the trailing edge region is an elliptic region of $O(R^{-\frac{3}{4}})$ and therefore a correct mathematical description must be based upon the full Navier–Stokes equations.

The 'method of series truncation' is used to reduce the full Navier–Stokes equations, written in parabolic co-ordinates, to an infinite set of non-linear, coupled, ordinary differential equations. Two sets of asymptotic boundary conditions, called simplified and exact boundary conditions, are determined by matching the Navier–Stokes region downstream with Goldstein's near wake solution.

By numerical integration the solutions for the first and second truncations are obtained for both sets of asymptotic boundary conditions. The results confirm that the size of the trailing edge region is of $O(R^{-\frac{3}{4}})$.

1. Introduction

The investigation reported in this paper is a theoretical study of the trailing edge region of a finite flat plate of length L in laminar, incompressible flow. The plate, which is of mathematical thickness zero, is aligned parallel to a flowing fluid of infinite extent, the undisturbed uniform velocity at infinity upstream being U_∞. It is assumed that the Reynolds number $R = U_\infty L/\nu$ is large so that a boundary layer exists downstream of the leading edge. With these assumptions boundary-layer theory gives a solution for the flow field along the flat plate, except for the region very close to the leading edge, and in the near wake, i.e. the Blasius solution and Goldstein's near wake solution, respectively.

It was shown by Blasius (1908) that the introduction of a new y co-ordinate, $\tilde{y} = (\tilde{y}_1/4\tilde{x}_1)((4U_\infty \tilde{x}_1/\nu)^{\frac{1}{2}})$ along with a new stream function, $\tilde{\psi}_1 = (U_\infty \nu \tilde{x}_1)^{\frac{1}{2}} f(\tilde{y})$, reduces the boundary-layer equation for the flat plate to the ordinary differential equation $f''' + ff'' = 0$ with boundary conditions $f(0) = f'(0) = 0$ and $f'(\infty) = 2$, where the velocity is given by $u = (u_1/U_\infty) = \frac{1}{2}f'$.

In Goldstein's (1930) analysis the assumption is made that at the trailing edge there exists a Blasius profile which is indistinguishable from the profile that would be found a distance L downstream from the leading edge of a semi-infinite flat plate; i.e. the flow along the plate up to the trailing edge is entirely

† Present address: IBM Research Laboratory, San Jose, California.

unaware of the flow beyond the trailing edge. This profile is taken to be the initial profile, and with due regard to the new boundary conditions the flow field in the near wake is obtained.

The theoretical results of the Blasius solution have been verified experimentally by Burgers (1924), Hansen (1930) and Nikuradse (1942); Goldstein's solution has been confirmed by measurements of Fage (1933) (Goldstein 1933, appendix) and of Grove, Petersen & Acrivos (1964). Thus, the above considerations suggest that the flow over the flat plate can be described fully on the basis of the boundary-layer equations. However, in the immediate neighbourhood of the trailing edge there is no reason why one of the essential assumptions of the boundary-layer theory, namely the assumption $\partial^2 u/\partial y^2 \gg \partial^2 u/\partial x^2$, should still hold. In a very small region, where the Blasius-type profile is changing into a wake-type profile, no information can be obtained with respect to the relative magnitude of $\partial^2 u/\partial x^2$ and $\partial^2 u/\partial y^2$. Therefore, $\partial^2 u/\partial x^2$ is to be retained together with $\partial^2 u/\partial y^2$ and, since a similar argument holds for the velocity component in the y direction, the appropriate equations describing the physical situation at the trailing edge are the full Navier–Stokes equations. Van Dyke (1967) seems to have been the first to indicate that the Navier–Stokes equations must be solved in this region.

In regions where the boundary-layer equations apply the transport mechanism consists of convection downstream and diffusion in the cross-stream direction. From a mathematical viewpoint the last statement expresses the fact that Prandtl's boundary-layer equations are parabolic. In such cases, the knowledge of initial conditions at $x_1 = 0$ is sufficient to determine completely the flow field for $x_1 > 0$. This means physically that disturbances spread downstream only, upstream influence being completely absent. If $\partial^2 u/\partial x^2$ is retained as well as $\partial^2 u/\partial y^2$, the transport mechanism consists of one additional effect—streamwise diffusion. In this case the equations are the Navier–Stokes equations, which are elliptic. The significance of this is that the flow slightly upstream of the trailing edge is not independent of that immediately downstream, disturbances are propagated upstream as well as downstream, and boundary conditions need to be specified all along the boundary.

It was indicated above by heuristic reasoning that the region, in which the full Navier–Stokes equations are to be solved, is confined to the immediate neighbourhood around the trailing edge. This situation can now be stated differently by saying that the elliptic region around the trailing edge is surrounded by a parabolic region, or, equivalently, the trailing edge is sheltered by the boundary layer.

Experimental and theoretical studies at low Reynolds numbers indicate that the shear stress increases as the rear end of the plate is approached. According to boundary-layer theory, the distribution of shear stress is approximately constant ($\sim 1/\sqrt{\tilde{x}_1}$) in the trailing edge region, and zero along the centreline of the wake. Since singular behaviour can be expected in the trailing edge region, questions of importance which arise are: (1) is the shear stress continuous or discontinuous at the trailing edge; (2) what is the nature of the relationship between the distribution of shear stress and Reynolds number; (3) how does the

region of influence depend on the Reynolds number? The theoretical and numerical calculations of the following sections are meant to be contributions toward answering these questions for large Reynolds numbers.

2. Review of existing theories for the trailing edge problem

In reviewing earlier work on the trailing edge problem, one finds that most previous attempts relied on either Prandtl's boundary-layer equations or Oseen-type equations, and that only very few authors have tried to treat the problem on the basis of the full Navier–Stokes equations.

One of the first attacks on this problem was Kuo's (1953) analysis, which is based on a perturbation of the boundary-layer equations. In considering the flow over a finite flat plate, Kuo assumed that the stream function ψ and the pressure p could be expanded in the form

$$\psi = \psi^{(0)} + \epsilon\psi^{(1)} + \epsilon^2\psi^{(2)} + \ldots,$$

and

$$p = p^{(0)} + \epsilon p^{(1)} + \epsilon^2 p^{(2)} + \ldots,$$

where $\epsilon = R^{-\frac{1}{2}}$ and $p^{(0)} \equiv 0$. It is clear that $\psi^{(0)}$ represents the Blasius solution. The first-order pressure is obtained by solving the problem of potential flow over a thin airfoil with a shape given by the displacement parabola along the flat plate followed by a cylindrical afterbody, since the displacement thickness is assumed to be constant in the wake. Once the perturbation pressure is known, the first-order equation for the stream function can be solved. The expression for the total drag coefficient of the finite flat plate is given by Kuo as $C_D = 1{\cdot}328 \times R^{-\frac{1}{2}} + 4{\cdot}12\,R^{-1}$, the second term representing the effect of the trailing edge. Although the drag contribution from the leading edge has not been taken into consideration in this analysis, and Van Dyke (1964*a*) questions the correctness of the factor 4·12,† the above result is found to be in very good agreement with experimental measurements. However, Kuo's perturbation equation for $\psi^{(1)}$ remains within the framework of boundary-layer theory, i.e. the term $\partial^2 u/\partial x^2$ is still neglected to the order of $\psi^{(1)}$. Consequently, the flow in the wake does not exert an upstream influence on the flat plate except through the slightly changed pressure distribution of the potential flow, and therefore the exact nature of the flow at the trailing edge does not seem to be given correctly.

A similar objection can be made with respect to the work of Goldburg & Cheng (1961), who attacked the trailing edge problem using the method of strained co-ordinates (PLK method). The same authors carried out a study of Goldstein's wake solution, and improved the solution by rewriting and solving the problem in parabolic co-ordinates. The PLK method predicts the region of influence to be proportional to $R^{-\frac{1}{2}}$, while the parabolic co-ordinate transformation yields R^{-1}. It will be shown later that the correct region of influence is proportional to $R^{-\frac{3}{4}}$; the discrepancy of Goldburg's results is most likely attributable to the use of boundary-layer equations, rather than the full Navier–Stokes equations.

† As the result of a subsequent re-examination of the series from which the value 4·12 is obtained, Van Dyke (1969, personal communication) has removed his objections to Kuo's original estimate of the size of this factor.

Whereas the boundary-layer equations are parabolic, the Oseen equations are elliptic, and it appears that these latter equations reflect much better the physical situation at the trailing edge, if the linearization is based on a velocity characteristic of this region. Since in the trailing edge region, close to the wall, the Blasius flow is similar to a shear flow (i.e. $u \sim |y|$ and $v \approx 0$), it seems reasonable to linearize the non-linear convection term $u(\partial u/\partial x)$ by $|y|(\partial u/\partial x)$. A slightly different linearization is obtained by assuming that the flow approaches a wake flow. In this case $u \sim y^2$, and the proper linearization is given by $y^2(\partial u/\partial x)$. A linearization of the second type has been employed by Cheng (1967), and linearizations of the first kind were used by Imai (1964) and Stewartson (1968). Although the mathematical solutions are involved and differ in detail, all three theories have in common that the linearized equations are Fourier-transformed and then solved by the Wiener–Hopf technique.

Imai assumes the pressure to be constant along the plate, which results in the boundary condition $(\partial/\partial y)(\nabla^2\psi) = 0$. Stewartson shows that this boundary condition is not justified, and replaces it by the exact condition $\psi = \partial\psi/\partial y = 0$ at $y = 0, x < 0$. From Stewartson's solution it is observed that the shear stress is discontinuous at the trailing edge, having an algebraic singularity there.

Results similar to Stewartson's were obtained in the numerical analysis by Dennis & Dunwoody (1966), using the full Navier–Stokes equations in elliptic co-ordinates. From this solution it is found that a singularity of the shear stress exists at the trailing edge. The predictions of boundary-layer theory are approached as the Reynolds number increases; the singularity is pushed more and more towards the trailing edge, and in the limit of very large Reynolds numbers only a point of discontinuity remains.

In §5 the solutions of Dennis & Dunwoody (1966), Imai (1964) and Stewartson (1968) will be taken up again, and a detailed comparison will be made with the solution developed in §§3 and 4.

Finally, the recent work of Davis (1967) on the semi-infinite flat plate should be mentioned. Davis uses the method of series truncation; our analysis of the trail-edge region is closely related to his.

3. Theoretical investigation of the flow near the trailing edge

3.1. *Flow régimes near the trailing edge*

In §2 the physical nature of the trailing edge was discussed, and it was suggested that the trailing edge is sheltered by the boundary layer. This assertion will now be strengthened by a mathematical analysis of the different flow régimes near the trailing edge.

If the origin of the co-ordinate system is taken at the trailing edge, with x_1 opposite to the oncoming stream and y_1 perpendicular to it, and if non-dimensional variables are introduced by

$$x = x_1/L, \quad y = y_1/L, \tag{3.1}$$

$$\psi = \psi_1/U_\infty L, \quad R = U_\infty L/\nu, \tag{3.2}$$

then the full Navier–Stokes equations can be written in terms of the stream function ψ as

$$[\psi_y(\partial/\partial x) - \psi_x(\partial/\partial y) - (1/R)\nabla^2]\nabla^2\psi = 0. \tag{3.3}$$

In the limit $R \to \infty$, (3.3) reduces to the inviscid Euler equation,

$$[\psi_y(\partial/\partial x) - \psi_x(\partial/\partial y)]\nabla^2\psi = 0. \tag{3.4}$$

For the present problem the flow at upstream infinity is irrotational and uniform, so that the solution of (3.4) is given by $\psi = y$. The region in which the Euler equation is valid will be called 'region I' (cf. figure 1). In the neighbourhood of the wall a non-uniformity exists, since the non-slip condition cannot be satisfied. This deficiency is corrected by redefining new variables, so called 'inner variables,' and then taking the limit $R \to \infty$. It was shown by Prandtl that the correct inner variables are $y = R^{-\frac{1}{2}}Y$ and $\psi = R^{-\frac{1}{2}}\Psi$, the other non-dimensional quantities remaining unchanged. In the new variables, (3.3) becomes

$$\left[\Psi_Y \frac{\partial}{\partial x} - \Psi_x \frac{\partial}{\partial Y} - \frac{1}{R}\left(\frac{\partial^2}{\partial x^2} + R\frac{\partial^2}{\partial Y^2}\right)\right]\left[\frac{\partial^2}{\partial x^2} + R\frac{\partial^2}{\partial Y^2}\right]\Psi = 0. \tag{3.5}$$

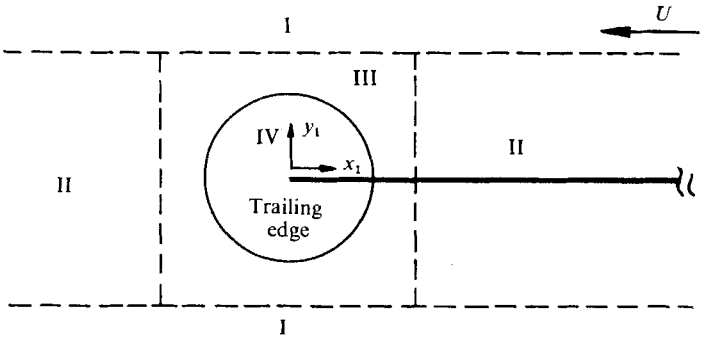

FIGURE 1. Flow régimes near the trailing edge.

If the limit $R \to \infty$ is now taken, the boundary-layer equations of Prandtl are obtained in the form,

$$\left[\Psi_Y \frac{\partial}{\partial x} - \Psi_x \frac{\partial}{\partial Y} - \frac{\partial^2}{\partial Y^2}\right]\left[\frac{\partial^2\Psi}{\partial Y^2}\right] = 0, \tag{3.6}$$

or after integration

$$\Psi_{YYY} + \Psi_x \cdot \Psi_{YY} - \Psi_Y \cdot \Psi_{xY} = -\Psi_Y(x, 0)\Psi_{xY}(x, 0). \tag{3.7}$$

The domain of validity of the boundary-layer equations will be called 'region II' (cf. figure 1).

It is obvious that the boundary-layer solution must fail at a distance of $O(R^{-\frac{1}{2}})$ from the trailing edge, because at this distance x becomes of the same order as y. To consider this region, x must be stretched by an amount $R^{-\frac{1}{2}}$ in addition to the boundary-layer variables; thus a new magnified x scale is introduced by defining $x = R^{-\frac{1}{2}}X$. With the new x variable (3.5) becomes

$$\left[\Psi_Y \frac{\partial}{\partial X} - \Psi_X \frac{\partial}{\partial Y} - \frac{1}{\sqrt{R}}\left(\frac{\partial^2}{\partial X^2} + \frac{\partial^2}{\partial Y^2}\right)\right]\left[\frac{\partial^2}{\partial X^2} + \frac{\partial^2}{\partial Y^2}\right]\Psi = 0, \tag{3.8}$$

and in the limit $R \to \infty$ this reduces to

$$\left[\Psi_Y \frac{\partial}{\partial X} - \Psi_X \frac{\partial}{\partial Y}\right]\left[\frac{\partial^2}{\partial X^2} + \frac{\partial^2}{\partial Y^2}\right]\Psi = 0. \tag{3.9}$$

Equation (3.9) is recognized as the Euler equation, which describes an inviscid region around the trailing edge. Because upstream of the trailing edge, the boundary-layer solution is valid, the above inviscid region, called henceforth 'region III', must match to it (cf. figure 1). Since close enough to the wall the Blasius flow behaves like a simple shear flow, the stream function in the inviscid region in the neighbourhood of the wall must vary as

$$\Psi \sim \tfrac{1}{2}Y^2. \tag{3.10}$$

Although the above inviscid solution is valid in a small region around the trailing edge, it fails in the immediate neighbourhood of the plate, and must be replaced by the Navier–Stokes solution. To find the extent of the Navier–Stokes region, which will be called 'region IV' (cf. figure 1), the following additional scaling is introduced:

$$x_{\mathrm{IV}} = R^{\alpha}X, \tag{3.11a}$$

$$y_{\mathrm{IV}} = R^{\alpha}Y, \tag{3.11b}$$

$$\psi_{\mathrm{IV}} = R^{\beta}\Psi, \tag{3.11c}$$

Equation (3.8) now becomes

$$\left[R^{-\beta}\frac{\partial\psi_{\mathrm{IV}}}{\partial y_{\mathrm{IV}}} - R^{-\beta}\frac{\partial\psi_{\mathrm{IV}}}{\partial x_{\mathrm{IV}}} - \frac{1}{R^{\frac{1}{2}}}\left(\frac{\partial^2}{\partial x_{\mathrm{IV}}^2} + \frac{\partial^2}{\partial y_{\mathrm{IV}}^2}\right)\right]\left[\frac{\partial^2}{\partial x_{\mathrm{IV}}^2} + \frac{\partial^2}{\partial y_{\mathrm{IV}}^2}\right]\psi_{\mathrm{IV}} = 0. \tag{3.12}$$

If (3.12) is to describe a Navier–Stokes régime, it is necessary that the limit process $R\to\infty$ leave the equation invariant. This condition is seen to be satisfied for $\beta = \frac{1}{2}$. In addition, as $y_{\mathrm{IV}}\to\infty$ the Navier–Stokes region must match to region III. Hence, the matching condition for region IV is found from (3.10) and, after rewriting in variables of region IV,

$$\lim_{y_{\mathrm{IV}}\to\infty} R^{-\beta}\psi_{\mathrm{IV}} \sim \tfrac{1}{2}R^{-2\alpha}y_{\mathrm{IV}}^2. \tag{3.13}$$

The last expression should not depend on the Reynolds number, thus leading to $\beta = 2\alpha$, and since $\beta = \frac{1}{2}$, it follows that $\alpha = \frac{1}{4}$. The correct scaling in the Navier–Stokes region is now found to be

$$x_{\mathrm{IV}} = R^{\frac{1}{4}}X, \tag{3.14}$$

$$y_{\mathrm{IV}} = R^{\frac{1}{4}}Y, \tag{3.15}$$

$$\psi_{\mathrm{IV}} = R^{\frac{1}{2}}\Psi. \tag{3.16}$$

In the original variables, this leads to

$$x_1/L = x = R^{-\frac{1}{2}}X = R^{-\frac{3}{4}}x_{\mathrm{IV}} \quad \text{and} \quad x_{\mathrm{IV}} = (x_1/L)R^{\frac{3}{4}}, \tag{3.17}$$

or

$$y_1/L = y = R^{-\frac{1}{2}}Y = R^{-\frac{3}{4}}y_{\mathrm{IV}} \quad \text{and} \quad y_{\mathrm{IV}} = (y_1/L)R^{\frac{3}{4}}. \tag{3.18}$$

Whereas the boundary-layer region is of $O(R^{-\frac{1}{2}})$, the Navier–Stokes region at the trailing edge is seen to be of $O(R^{-\frac{3}{4}})$. This estimate, first recognized by Van Dyke (1967), Stewartson (1968)' and Riley'(1968, unpublished), implies that the region of non-uniformity at the trailing edge is much smaller than the extent of the boundary layer, confirming the earlier statement describing the trailing edge as being sheltered by the boundary layer.

The discussion above is valid for more general trailing edges than that of a flat plate. Although in general a region III exists, it should be pointed out that for the special case of a flat plate, because there is neither creation nor diffusion of vorticity in the inviscid region, the only role of region III here is to convect the Blasius profile undistorted downstream from the boundary-layer region to the Navier–Stokes region.

As the Reynolds number increases, the Navier–Stokes region decreases. Therefore Goldstein's assumption of a Blasius profile at the trailing edge is the appropriate initial profile for the near wake solution and, in addition, it would appear to be valid to utilize the Goldstein solution as the downstream boundary condition in determining the flow field in the interior of the Navier–Stokes region.

3.2. *Navier–Stokes equations in parabolic co-ordinates*

If the flow over the flat plate is described in Cartesian x_1, y_1 co-ordinates, the boundary conditions are discontinuous along the line $y_1 = 0$. This discontinuity causes the flow to be singular in the trailing edge region, and in addition it renders the mathematical analysis much more difficult. A co-ordinate system, which takes better account of the physical situation, is the parabolic co-ordinate system, defined by

$$x_1 = (\nu/2U_\infty)(\xi^2-\eta^2), \tag{3.19}$$

$$y_1 = (\nu/U_\infty)\xi\eta. \tag{3.20}$$

(Throughout the paper the subscript 1 will denote dimensional co-ordinates.) In the transformed co-ordinates the flat plate corresponds to $\eta = 0$, while the centreline of the wake is given by $\xi = 0$. Although a discontinuity in the boundary conditions still exists, the new co-ordinates have the advantage that the whole plate and nothing else is described by $\eta = 0$. The discontinuity introduced at the leading edge is irrelevant for the consideration of the trailing edge region, since it corresponds to infinity upstream. In terms of a non-dimensional stream function, defined by $\psi = (\psi_1/\nu)$, the full Navier–Stokes equations can now be written in the form

$$\left[\left(\frac{\partial^2}{\partial\xi^2}+\frac{\partial^2}{\partial\eta^2}\right)+\frac{\partial\psi}{\partial\xi}\frac{\partial}{\partial\eta}-\frac{\partial\psi}{\partial\eta}\frac{\partial}{\partial\xi}\right]\left[\left(\frac{\partial^2\psi}{\partial\xi^2}+\frac{\partial^2\psi}{\partial\eta^2}\right)\Big/(\xi^2+\eta^2)\right] = 0. \tag{3.21}$$

3.3. *Asymptotic boundary conditions*

In §3.1 it was established that Goldstein's near wake solution is the appropriate downstream boundary condition for the trailing edge region, the upstream boundary condition being the Blasius solution. This line of development will now be pursued further, resulting in the formulation of the asymptotic boundary conditions far downstream. In doing so we shall formulate simplified and exact boundary conditions: the former express the condition that the solution in the Navier–Stokes region 'patch' to the Goldstein solution at some asymptotic distance, whereas the exact boundary conditions require that the two solutions have the same functional form asymptotically, i.e. that they 'match'. Although the latter are obviously the proper ones to impose, we include the simplified ones because they are computationally the easier to apply, and so permit the

clearest exposition of the method of solution; furthermore, they allow a useful comparison to be made between the solutions obtained with each of the sets of boundary conditions. As we shall see when we discuss the solutions, in at least one important result, the solutions with the simplified boundary conditions are in remarkable agreement with the exact boundary condition solutions.

3.3.1. *Simplified boundary conditions.* Expanding the velocity profiles in the near wake in a Taylor series, one obtains

$$u = c_0 + c_2\bar{y}^2 + c_4\bar{y}^4 + \ldots, \tag{3.22}$$

where the coefficients $c_0, c_2, c_4, \ldots$, are obtained from Goldstein's solution and $\bar{y} = (y_1/4L)((4U_\infty L/\nu)^{\frac{1}{2}})$. If one defines $\psi_1 = \int u_1 dy_1$, (3.22) becomes after integrating

$$\psi = \frac{\psi_1}{\nu} = c_0\xi\eta + \frac{c_2}{12U_\infty L/\nu}\xi^3\eta^3 + \frac{c_4}{80(U_\infty L/\nu)^2}\xi^5\eta^5 + \ldots. \tag{3.23}$$

This last expression is meant to be an approximation to Goldstein's stream function, and must be matched asymptotically by the stream function of the Navier–Stokes region. Therefore, (3.23) is seen to represent the asymptotic boundary conditions to be satisfied by the stream function of the Navier–Stokes region in the limit of large η. Although in the derivation of (3.23) the dependence of the coefficients $c_0, c_2, c_4, \ldots$, on the axial distance x_1 is neglected, consideration of this point will be given in the matching process to be discussed in §4.2.3.

3.3.2. *Exact boundary conditions.* Whereas the simplified boundary conditions are based on an approximation to Goldstein's stream function, the 'exact' boundary conditions to be derived in this section rely on the exact expression of Goldstein's stream function, which, close to the axis, is given by

$$\begin{aligned}\bar{\psi} = {} & \bar{\xi}^2\left(\beta_0\bar{\eta} + \beta_0^2\frac{\bar{\eta}^3}{3!} - 2\beta_0^3\frac{\bar{\eta}^5}{5!} + 10\beta_0^4\frac{\bar{\eta}^7}{7!} + \ldots\right) \\ & + \bar{\xi}^5\left[\beta_3\left(\bar{\eta} + 5\beta_0\frac{\bar{\eta}^3}{3!} + 40\beta_0^3\frac{\bar{\eta}^7}{7!} - 160\beta_0^4\frac{\bar{\eta}^9}{9!} + \ldots\right)\right] \\ & + \bar{\xi}^8\left[\beta_3^2\left(4\frac{\bar{\eta}^3}{3!} + 6\beta_0\frac{\bar{\eta}^5}{5!} + 132\beta_0^2\frac{\bar{\eta}^7}{7!} + \ldots\right)\right. \\ & \left. + \beta_6\left(\bar{\eta} + 8\beta_0\frac{\bar{\eta}^3}{3!} + 24\beta_0^2\frac{\bar{\eta}^5}{5!} + 112\beta_0^3\frac{\bar{\eta}^7}{7!} + \ldots\right)\right].\end{aligned} \tag{3.24}$$

The non-dimensional variables in (3.24) are defined as $u = (\partial\bar{\psi}/\partial\bar{y})$, $\bar{x} = (\bar{x}_1/4L)$, $\bar{y} = (y_1/4L)((4U_\infty L/\nu)^{\frac{1}{2}})$, $u = (u_1/U_\infty)$ and $v = (v_1/U_\infty)((4U_\infty L/\nu)^{\frac{1}{2}})$, the co-ordinate system being located at the trailing edge, with $\bar{x}$ and u increasing in the downstream direction. The variables $\bar{\xi}, \bar{\eta}$ are related to the parabolic co-ordinates ξ, η by

$$\bar{\xi} = a(\eta^2 - \xi^2)^{\frac{1}{3}} \quad (a = 1/(2R^{\frac{1}{3}})), \tag{3.25}$$

and

$$\bar{\eta} = b[\xi\eta/(\eta^2 - \xi^2)^{\frac{1}{3}}] \quad (b = 1/(3R^{\frac{1}{6}})), \tag{3.26}$$

and the stream functions by $\psi = 2R^{\frac{1}{2}}\bar{\psi}$. (Bars over quantities are used to denote variables in the Goldstein solution, whose definition differs from that used elsewhere in the paper for similar quantities. Note, for example, that $\bar{x}_1 = -x_1$.)

Values on or near the centreline of the wake are considered by holding η fixed and letting $\xi \to 0$. Thus (3.24) becomes, after rewriting in parabolic co-ordinates and expanding for small values of ξ,

$$\begin{aligned}\psi = \xi\left[\frac{a\beta_0}{3}\eta^{\frac{5}{3}} + \frac{a^4\beta_3}{3}\eta^{\frac{11}{3}} + \frac{a^7\beta_6}{3}\eta^{\frac{17}{3}} + \ldots\right] \\ + \xi^3\left[-\frac{a\beta_0}{9}\eta^{-\frac{1}{3}} + \frac{ab^2\beta_0^2}{18}\eta^{\frac{7}{3}} - \frac{4a^4\beta_3}{9}\eta^{\frac{5}{3}} + \frac{5a^4\beta_3\beta_0 b^2}{18}\eta^{\frac{13}{3}}\right. \\ \left. - \frac{7a^7\beta_6}{9}\eta^{\frac{11}{3}} + \frac{2a^7b^2\beta_3^2}{9}\eta^{\frac{19}{3}} + \ldots\right] + \xi^5\left[\frac{2a\beta_0}{27}\eta^{-\frac{7}{3}} + \ldots\right]. \qquad (3.27)\end{aligned}$$

Since the stream function of the Navier–Stokes region must match asymptotically to Goldstein's stream function, (3.27) represents the asymptotic boundary condition to be satisfied by the stream function of the Navier–Stokes region in the limit as $\eta \to \infty$.

4. Mathematical and numerical solution of the trailing edge problem by the method of series truncation

4.1. *Asymptotic expansion of the full Navier–Stokes equations*

To solve the Navier–Stokes equations in the trailing edge region, we shall employ the 'method of series truncation', pioneered by Van Dyke (1964*b*, 1965) and his students at Stanford. The essential idea of the method is to treat an elliptic partial differential equation as if it were parabolic or hyperbolic; i.e. the solution is expanded in powers of one co-ordinate, which plays the role of a time-like variable. Substitution of the series into the governing equations and equating like powers of the downstream variable yields a sequence of ordinary differential equations in which at any stage the number of unknowns exceeds the number of equations. The resulting indeterminacy is removed by truncating the series in some manner. It is assumed that as the order of the system is increased the corresponding solution tends to the exact solution. Although there is as yet no formal mathematical justification for the method, and its main applicability might seem to be for problems with weak backward influence, Van Dyke (1964*b*, 1965) has shown that series truncation can be applied with reasonable success even to highly elliptic problems, if the variables are judiciously chosen.

The asymptotic boundary conditions, derived in the previous section, suggest an expansion of ψ in the form,

$$\psi = -\sum_{n=1}^{\infty} \xi^{2n-1} f_n(\eta) = -\xi f_1(\eta) - \xi^3 f_2(\eta) - \xi^5 f_3(\eta) + \ldots. \qquad (4.1)$$

Introducing (4.1) into the full Navier–Stokes equations, expressed in parabolic

co-ordinates, and equating equal powers of ξ results in a system of non-linear, coupled ordinary differential equations of fourth order, given below.

$$\eta f_1^{\mathrm{IV}} - 4f_1''' + 12\eta f_2'' - 24f_2' + 120\eta f_3 - 6\eta f_1 f_2' - \eta f_1 f_1''' + 12 f_1 f_2 + 2 f_1 f_1'' + 6\eta f_1' f_2 + \eta f_1' f_1'' = 0, \tag{4.2a}$$

$$-2\eta f_1^{\mathrm{IV}} + 4f_1''' - \eta^3 f_2^{\mathrm{IV}} + 4\eta^2 f_2''' - 16\eta f_2'' + 24 f_2' - 40\eta^3 f_3'' + 80\eta^2 f_3' - 80\eta f_3 - 2 f_1 f_1'' + 2\eta f_1 f_1''' - 12 f_1 f_2 + 12\eta f_1 f_2' + 20\eta^3 f_1 f_3' - 40\eta^2 f_1 f_3 - 2\eta^2 f_1 f_2'' + \eta^3 f_1 f_2''' - 3\eta^3 f_1' f_2'' - 60\eta^3 f_1' f_3 - \eta^3 f_1'' f_2' - 6\eta^2 f_1'' f_2 + 3\eta^3 f_1''' f_2 - 36\eta^2 f_2^2 + 12\eta^3 f_2 f_2' = 0, \tag{4.2b}$$

$$-f_1^{\mathrm{IV}} - 2\eta^2 f_2^{\mathrm{IV}} + 4\eta f_2''' - 4f_2'' - \eta^4 f_3^{\mathrm{IV}} + 4\eta^3 f_3''' - 64 f_3''\eta^2 + 80\eta f_3' + 40 f_3 + \eta^4 f_1 f_3''' + 40\eta^2 f_1 f_3' + 2\eta^2 f_1 f_2''' + 6 f_1 f_2' + f_1 f_1''' + 54\eta^4 f_2 f_3' + 3\eta^4 f_2 f_2''' + 36\eta^2 f_2' f_2 + 6\eta^2 f_2 f_1''' - 30\eta^4 f_3 f_2' + 5\eta^4 f_3 f_1''' - 2\eta^3 f_1 f_3'' - 40\eta f_1 f_3 - 2\eta f_1 f_2'' - 5\eta^4 f_1' f_3'' - 80\eta^2 f_1' f_3 - 4\eta^2 f_1' f_2'' + 6 f_1' f_2 + f_1' f_1'' - 3\eta^4 f_2' f_2'' - \eta^4 f_3' f_1'' - 36\eta f_2^2 - 6\eta f_1'' f_2 - 180\eta^3 f_2 f_3 - 6\eta^3 f_2 f_2'' - 10\eta^3 f_3 f_1'' = 0, \tag{4.2c}$$

... ...

It can be observed that in the first equation (4.2a), not only the function f_1 and its derivatives occur, but also f_2 and f_3 and their derivatives. This is a property not only of the lowest order equation, but also of all subsequent equations, and therefore at each step of the approximation the number of unknowns exceeds the number of equations.

A solution of the system (4.2a–c, ...) is made possible by truncating the series. In the first truncation, this consists of setting $f_2, f_3, \ldots$, and their derivatives equal to zero, and solving the simplified equation (4.2a). For the second truncation, the terms $f_3, f_4, \ldots$, as well as their derivatives, are assumed to be zero, and a solution of (4.2a) and (4.2b) must be found simultaneously. Since (4.2a) takes on different forms under the assumptions of the first and second truncations, none of the information contained in the solution of the first truncation can be used in obtaining the solution of the second truncation. The third truncation consists of solving (4.2a–c) simultaneously, the terms of order $f_4, f_5, \ldots$ and all their derivatives being neglected.

The boundary conditions along the plate are

$$\psi_1(x_1, y_1)|_{y_1=0} = \psi_1(x_1, 0) = \psi(\xi, 0) = 0$$

and

$$u_1 = \frac{\partial \psi_1}{\partial y_1}\bigg|_{y_1=0} = \nu \left(\frac{\partial \psi}{\partial \eta}\frac{\partial \eta}{\partial y_1} + \frac{\partial \psi}{\partial \xi}\frac{\partial \xi}{\partial y_1} \right)\bigg|_{\eta=0} = 0.$$

By (4.1) this is equivalent to

$$f_1(0) = f_2(0) = f_3(0) = \ldots = 0 \tag{4.3}$$

and

$$f_1'(0) = f_2'(0) = f_3'(0) = \ldots = 0. \tag{4.4}$$

The asymptotic form of the boundary conditions far downstream is given by (3.23) and (3.27). On comparing with (4.1), the simplified boundary conditions require

$$\lim_{\eta\to\infty} f_1(\eta) = -(\ )\eta, \tag{4.5a}$$

$$\lim_{\eta\to\infty} f_2(\eta) = -(\ )\eta^3, \tag{4.5b}$$

$$\lim_{\eta\to\infty} f_3(\eta) = -(\ )\eta^5, \tag{4.5c}$$

... ...

whereas the exact boundary conditions demand

$$\lim_{\eta\to\infty} f_1(\eta) = -\frac{a}{3}\eta^{\frac{5}{3}}(\beta_0+\beta_3 a^3\eta^2+\ldots), \tag{4.6a}$$

$$\lim_{\eta\to\infty} f_2(\eta) = \tfrac{1}{9}\beta_0 a\eta^{-\frac{1}{3}} - \tfrac{1}{18}ab^2\beta_0^2\eta^{\frac{7}{3}} + \tfrac{4}{9}a^4\beta_3\eta^{\frac{5}{3}} - \tfrac{5}{18}a^4\beta_3\beta_0 b^2\eta^{\frac{13}{3}}+\ldots, \tag{4.6b}$$

$$\lim_{\eta\to\infty} f_3(\eta) = -\frac{2a\beta_0}{27}\eta^{-\frac{7}{3}}+\ldots, \tag{4.6c}$$

... ...

In (4.5*a–c*) and hereafter, open parentheses stand for constants which are unknown at this stage, but are determined as part of the solution.

Equations (4.2*a–c*), subject to the plate boundary conditions (4.3), (4.4), and either the asymptotic boundary conditions (4.5*a–c*) or (4.6*a–c*), describe the problem whose discussion will occupy the remaining part of § 4. It should be noted that in requiring that the series truncation solution satisfy boundary conditions at the plate and asymptotically far downstream, we are applying the method of series truncation in an unorthodox way. Inmost applications of the method integration proceeds upstream, the unstated premise being that one should swim against the 'current' as fast as possible, so as to minimize the effects of upstream influence (Van Dyke 1968, personal communication). However, as far as the authors are aware, there is no mathematical justification for assuming that the integration must always proceed upstream when using series truncation. Moreover, the use of parabolic co-ordinates, and the results of the solution of most interest to us, suggest that the direction of integration chosen here might be most appropriate. In particular, we are mostly interested in the shear stress distribution on the plate near the trailing edge and the extent of upstream influence of the trailing edge on the Blasius-boundary layer. By placing the ends of the integration for each on the $f_i(\eta)$ equations at the plate surface and the wake downstream, we are, in a sense, most directly allowing for the influence of the end of the plate to make itself felt on upstream plate quantities, and it is this influence which is the essence of the problem. In addition, imposing our 'far' boundary condition downstream, rather than upstream, allows us, without prejudice, to estimate the extent of upstream influence as the place where the solution matches (or patches) to the Blasius solution. (Although the Navier–Stokes region is elliptic, and hence the domain of influence is the same in all directions, it is more physically satisfying to define it in terms of the change in the upstream Blasius profile.)

Once the differential equations (4.2*a–c*) are solved, the distribution of the skin

friction at the trailing edge can be calculated from (4.1) using the definition of the skin friction; this yields

$$\tau = -\rho U_\infty^2 \left[\frac{f_1''(0)}{(2(x_1/L)\,R)^{\frac{1}{2}}} + f_2''(0)\,(2(x_1/L)\,R)^{\frac{1}{2}} + f_3''(0)\,(2(x_1/L)\,R)^{\frac{1}{2}})^3 + \ldots \right]. \quad (4.7)$$

4.2. *First truncation*

4.2.1. *Derivation and integration of the first truncation.* The first truncation requires the solution of the differential equation,

$$\eta f_1^{\mathrm{IV}} - 4f_1''' - \eta f_1 f_1''' + 2f_1 f_1'' + \eta f_1' f_1'' = 0. \quad (4.8)$$

The associated boundary conditions are, at $\eta = 0$,

$$f_1(0) = 0, \quad f_1'(0) = 0 \quad (4.9a,b)$$

and for large η, either

$$f_1(\eta) = -(\ )\eta \quad \text{(simplified boundary conditions)} \quad (4.9c)$$

or $$f_1(\eta) = -\tfrac{1}{3}a\eta^{\frac{5}{3}}(\beta_0 + \beta_3 a^3\eta^2 + \ldots) \quad \text{(exact boundary conditions)}. \quad (4.9d)$$

In general, two-point boundary value problems of the above type can be solved as initial value problems by starting the integration at $\eta = 0$, and determining the derivatives at $\eta = 0$ so as to satisfy the asymptotic boundary conditions for large values of η. However, the numerical integration of (4.8) cannot begin at the origin because the highest derivative is multiplied by η. One must then obtain a local analytic solution; in this case a Taylor series expansion is found to exist around $\eta = 0$, given by

$$f_1 = a_2\eta^2 + \tfrac{1}{15}a_2^2\eta^5 + a_7\eta^7 - \tfrac{17}{2520}a_2^3\eta^8 - \tfrac{1}{120}a_2 a_7\eta^{10} + \ldots. \quad (4.10)$$

Two arbitrary constants, a_2 and a_7, occur in (4.10). They are determined from the integral curves satisfying the asymptotic conditions, (4.9*c*) or (4.9*d*). To find this solution the integration was performed by fixing a_2 and varying a_7 over a large range of values. The integration was carried out using a fifth-order Runge–Kutta scheme. (The details of the numerical analysis are given in Talke 1968.) A typical set of integral curves for a particular choice of a_2 is shown in figure 2.

4.2.2. *Simplified boundary conditions.* From figure 2 it can be seen that for almost all values of a_7 the integral solutions and their derivatives become unbounded for large η. However, the character of the curves changes as a_7 ranges from negative to positive values. For large negative a_7 the integral curves and their derivatives are negative for all η, whereas they go through zero for positive a_7. Thus, a solution curve proportional to $-\eta$ for large η can be found only between the 'negative' and 'positive' integral curves. Since (4.8) reduces to an identity on introducing $f_1 \sim -k_1\eta$, $f_1' \sim -k_1$, $f_1'' = f_1''' = f_1^{\mathrm{IV}} = 0$, the differential equation is seen to be satisfied asymptotically by $f_1 \sim -k_1\eta$. Therefore, a solution to the differential equation (4.8) subject to (4.9*c*) exists and can be obtained as follows. The arithmetic mean of the a_7 values leading to the 'positive' and 'negative' solutions is formed, and the integration is carried out again. The a_7 of the

resulting integral curve, which is either 'positive' or 'negative' is then combined with the a_7 of the closest integral curve of opposite 'sign', and a new mean value a_7 is calculated; this procedure is repeated until numerical convergence is obtained (cf. figure 3). Only one solution needs to be determined by iteration because the differential equation (4.8) as well as the boundary conditions (4.9*a–c*) are invariant under the transformation,

$$f_1(\eta) \to cF(c\eta), \quad \eta \to (1/c)\eta. \tag{4.11}$$

Thus $f_1(\eta)$ can be determined from $F(c\eta)$, since $f_1''(0) = c^3 F_1''(0)$, and therefore

$$c = \left[\frac{f_1''(0)}{F_1''(0)}\right]^{\frac{1}{3}}. \tag{4.12}$$

The solution curves as a function of the parameter a_2 are shown in figure 4.

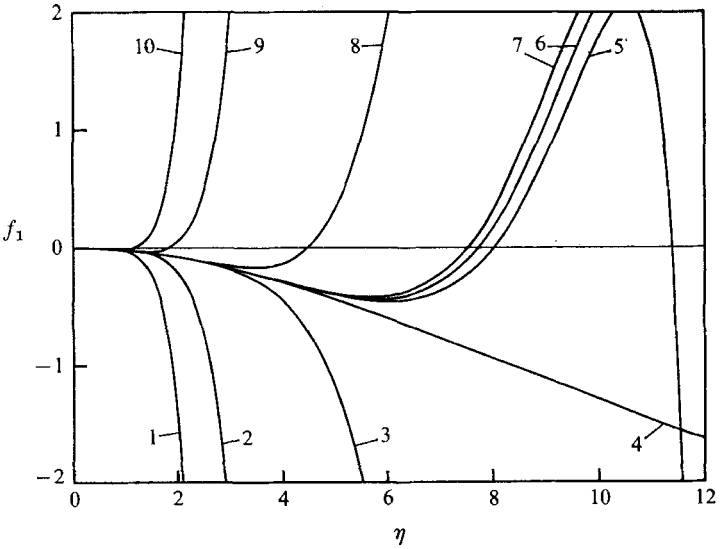

FIGURE 2. Integral curves for the first truncation:
$a_2 = -0{\cdot}02$

1	$a_7 = -0{\cdot}1 \times 10^{-1}$	6	$a_7 = 0{\cdot}0$
2	$a_7 = -0{\cdot}1 \times 10^{-2}$	7	$a_7 = 0{\cdot}1 \times 10^{-6}$
3	$a_7 = -0{\cdot}1 \times 10^{-4}$	8	$a_7 = 0{\cdot}1 \times 10^{-4}$
4	$a_7 = -0{\cdot}654 \times 10^{-6}$	9	$a_7 = 0{\cdot}1 \times 10^{-2}$
5	$a_7 = -0{\cdot}1 \times 10^{-6}$	10	$a_7 = 0{\cdot}1 \times 10^{-1}$

It was pointed out in §3.3 that the simplified boundary conditions are based on an approximation to Goldstein's near-wake stream function. In addition, the x variation of the coefficients $c_0, c_2, c_4, \ldots$ is neglected, and therefore the solution does not match asymptotically to Goldstein's solution. This deficiency can be corrected by demanding that the Navier–Stokes solution match numerically, i.e. patch, for large η with Goldstein's solution at some distance downstream, say $\bar{x}_{1\mathrm{M}}/L$, i.e.

$$\psi = -\xi f_1 = c_0 \xi \eta \quad \text{at} \quad \bar{x}_{1\mathrm{M}}/L,$$

or equivalently

$$f_1 = -c_0\eta \quad \text{at} \quad \eta = \eta_{\mathrm{M}}. \tag{4.13}$$

The non-dimensional distance $\bar{x}_{1\mathrm{M}}/L$, at which the numerical matching is enforced, is found by assuming that the value and the axial variation of the

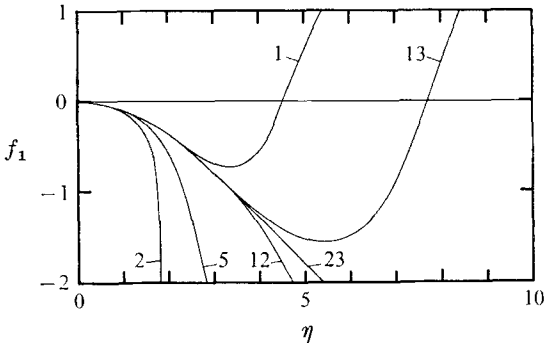

FIGURE 3. First truncation (simplified boundary conditions). Iteration on a_7. Number on curve represents number of iteration.

	$a_2 = -0{\cdot}1$	12	$a_7 = -0{\cdot}488 \times 10^{-4}$
1	$a_7 = -10^{-7}$	13	$a_7 = -0{\cdot}4395 \times 10^{-4}$
2	$a_7 = -10^{-2}$	23	$a_7 = -0{\cdot}47744 \times 10^{-4}$
5	$a_7 = -0{\cdot}125 \times 10^{-2}$		

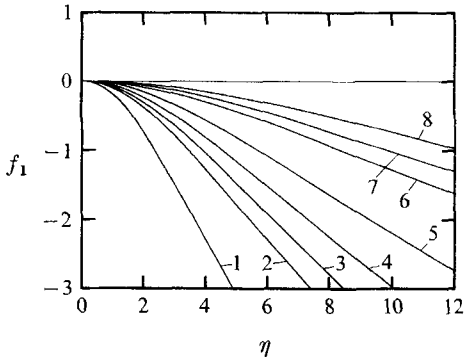

FIGURE 4. Solution curves for the first truncation (simplified boundary conditions):

1	$a_2 = -0{\cdot}200$	5	$a_2 = -0{\cdot}040$
2	$a_2 = -0{\cdot}100$	6	$a_2 = -0{\cdot}020$
3	$a_2 = -0{\cdot}080$	7	$a_2 = -0{\cdot}015$
4	$a_2 = -0{\cdot}060$	8	$a_2 = -0{\cdot}010$

centreline velocity distribution must be identical with Goldstein's solution in the neighbourhood of $\bar{x}_{1\mathrm{M}}/L$. The centreline velocity is obtained from (4.1) as

$$\left.\begin{aligned} u_{1c} &= \frac{\partial \psi_1}{\partial y_1} = \nu\left(\frac{\partial \psi}{\partial \xi}\frac{\partial \xi}{\partial y_1} + \frac{\partial \psi}{\partial \eta}\frac{\partial \eta}{\partial y_1}\right), \\ u_c &= -f(\eta)/\eta. \end{aligned}\right\} \tag{4.14}$$

Since $u_c = c_0$ at the matching station, condition (4.13) is seen to be contained in (4.14). Therefore, the numerical matching condition for the Navier–Stokes and Goldstein solution is the requirement that the value and the axial distribution of the centreline velocity be identical in the region close to $\bar{x}_{1\mathrm{M}}/L$ (corresponding to a particular value of η_{M}). Once $\bar{x}_{1\mathrm{M}}/L$ and η_{M} are determined (by graphical interpolation) such that the above condition is satisfied, the Reynolds number is found from (3.19) as

$$R = \eta_{\mathrm{M}}^2/[2(\bar{x}_{1\mathrm{M}}/L)]. \tag{4.15}$$

Thus, the matching process determines for each solution curve the station $\bar{x}_{1\mathrm{M}}/L$ at which the best agreement of the velocity distribution with Goldstein's solution is obtained. In this way the matching establishes the size of the Navier–Stokes region. It is found that $\bar{x}_{1\mathrm{M}}/L$ increases as the Reynolds number decreases ($\bar{x}_{1\mathrm{M}}/L = 0{\cdot}089$ for $R = 276$), whereas in the limit of high Reynolds numbers $\bar{x}_{1\mathrm{M}}/L$ becomes very small ($\bar{x}_{1\mathrm{M}}/L \sim 0{\cdot}001$ for $R = 65{,}600$). These results are in good agreement with earlier considerations: the Navier–Stokes region, being of $O(R^{-\frac{3}{4}})$, grows as the Reynolds number decreases, and therefore the appropriate boundary condition is applied 'far' from the trailing edge. As the Reynolds number increases, the Navier–Stokes region shrinks, the trailing edge is influenced only by its immediate neighbourhood, and the appropriate boundary condition is applied 'close' to the trailing edge.

As a result of the matching process a one-to-one correspondence is obtained between solution curves and Reynolds numbers, i.e. each solution corresponds to a unique Reynolds number.

4.2.3. *Exact boundary conditions.* We now consider the solution of the differential equation (4.8) subject to boundary conditions (4.9*a*), (4.9*b*) and (4.9*d*). From (4.9*d*) it can be seen that all solution curves become unbounded as $\eta \to \infty$. Furthermore, higher order terms, neglected in the derivation of (4.9) as well as in Goldstein's theory, begin to dominate in the limit of very large η. Clearly, the problem as formulated diverges and loses its physical meaning as $\eta \to \infty$. Therefore, the solution must be sought in a region where η is small enough so as to ensure the validity of neglecting the higher order terms. At the same time, η must be large enough to admit asymptotic behaviour of the solution. With these assumptions the correct 'asymptotic' boundary condition is found from (4.9*d*) as

$$f_1 = -(\tfrac{1}{3}\beta_0 a)\eta^{\frac{5}{3}}, \tag{4.16a}$$

or equivalently

$$R = \{-\tfrac{1}{6}\beta_0[1/(f_1/\eta^{\frac{5}{3}})]\}^3. \tag{4.16b}$$

By numerical integration of the differential equation, employing an iteration technique similar to the one described in the last section, a solution can be found satisfying the boundary conditions in a region $3 \lesssim \eta \lesssim 6$ for small Reynolds numbers and in $4 \lesssim \eta \lesssim 12$ for high Reynolds numbers. Thus the solution is obtained for values of η at which the matching of the simplified boundary conditions was carried out.

A graph of the solution curves satisfying the exact boundary conditions (4.16*a* or *b*) is to be found in figure 5. As with the simplified boundary conditions,

a one-to-one correspondence between solution curve and Reynolds number is thus established.

4.2.4. *Distribution of skin friction and region of influence.* The skin friction defined as $\frac{1}{2}c_f = \tau/(\rho U_\infty^2)$ is obtained for the trailing edge region from (4.7) by setting $f_2 = f_2' = \ldots f_3 = \ldots = 0$; thus

$$\tfrac{1}{2}c_f = -\left[\frac{f_1''(0)}{(2(x_1/L)\,R)^{\frac{1}{2}}}\right]. \tag{4.17}$$

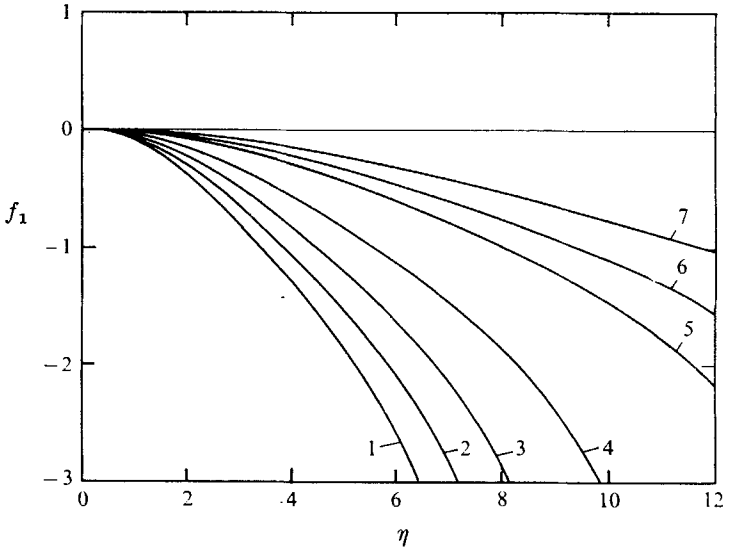

FIGURE 5. Solution curves for the first truncation (exact boundary conditions):

1	$a_2 = -0{\cdot}100$	5	$a_2 = -0{\cdot}020$
2	$a_2 = -0{\cdot}080$	6	$a_2 = -0{\cdot}015$
3	$a_2 = -0{\cdot}060$	7	$a_2 = -0{\cdot}010$
4	$a_2 = -0{\cdot}040$		

In figures 6 and 7 the distribution of the skin friction coefficient as a function of the Reynolds number is shown. It is observed that the skin friction is infinite at the trailing edge. Furthermore, the singularity of c_f grows as the Reynolds number decreases. Thus, the prediction of boundary-layer theory is seen to be approached nicely for large Reynolds numbers.

At some distance upstream of the trailing edge, say x_{1R}/L, the value of the skin friction is equal to the value of the skin friction as calculated from boundary-layer theory. This distance is assumed to represent the region of influence of the trailing edge, i.e. the region where the boundary-layer theory breaks down.

From the Blasius solution, the skin friction is calculated as

$$\tfrac{1}{2}c_f = \frac{0{\cdot}332}{(U\tilde{x}_1/L)^{\frac{1}{2}}}. \tag{4.18}$$

($\tilde{x}_1$ is distance along the plate measured from the leading edge). At x_{1R}/L this

must be equal to (4.17), and noting that $x_{1R} = L - \tilde{x}_{1R}$, the region of influence is obtained as

$$\frac{x_{1R}}{L} = \frac{[f_1''(0)]^2}{[f_1''(0)]^2 + 2[0{\cdot}332]^2}. \tag{4.19}$$

If the region of influence is calculated for different Reynolds numbers from (4.19), and the result is plotted as $\ln(x_{1R}/L)$ *versus* $\ln R$ (figures 8 and 9), it is

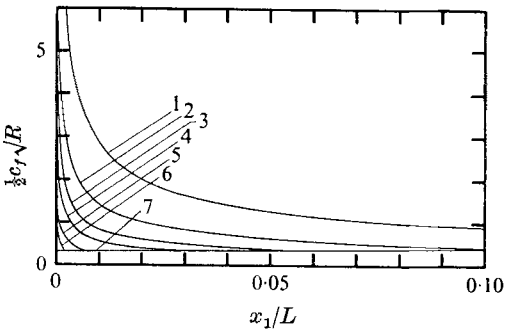

FIGURE 6. Distribution of skin friction at the trailing edge. First truncation (simplified boundary conditions):

1	R = 20	5	R = 10,900
2	R = 152	6	R = 65,600
3	R = 617	7	Blasius solution
4	R = 1810		

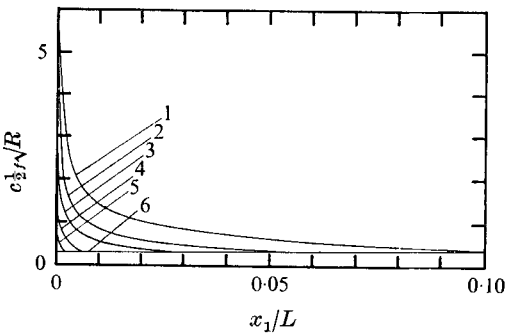

FIGURE 7 Distribution of skin friction at the trailing edge. First truncation (exact boundary conditions):

1	R = 106	4	R = 7,790
2	R = 411	5	R = 50,000
3	R = 1220	6	Blasius solution

found that all points lie on a straight line with the slope $m = -0{\cdot}747$ (simplified boundary conditions, cf. figure 8) and $m = -0{\cdot}74$ (exact boundary conditions, cf. figure 9). Thus the relationship between the region of influence and the Reynolds number is obtained for the simplified boundary conditions as

$$(x_{1R}/L) \sim R^{-0{\cdot}747}, \tag{4.20a}$$

and for the exact boundary conditions as

$$(x_{1R}/L) \sim R^{-0{\cdot}74}. \tag{4.20b}$$

The results (4.20*a*) and (4.20*b*) are in excellent agreement with the order of magnitude arguments of §3.1, which led to the prediction that the region of influence should be proportional to $R^{-\frac{3}{4}}$.

Further discussion of the first truncation will be postponed until §5; the remaining part of §4 is devoted to the solution of the second truncation.

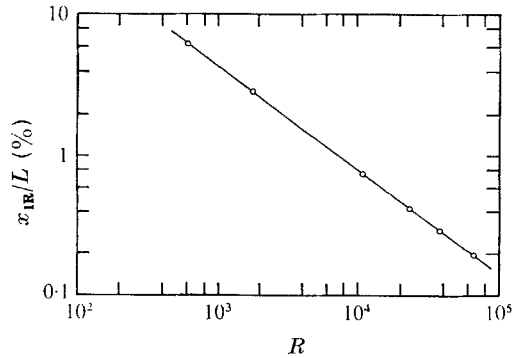

FIGURE 8. Region of influence *vs.* Reynolds number for the first truncation (simplified boundary conditions). Slope of the straight line: $m = -0{\cdot}747$.

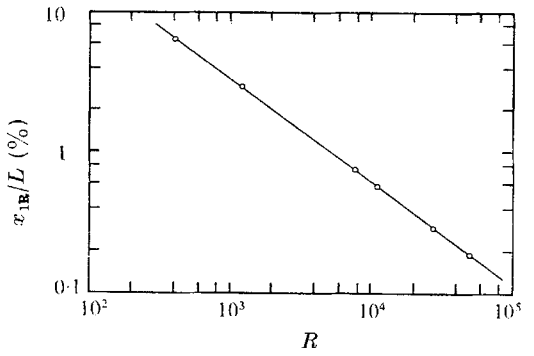

FIGURE 9. Region of influence *vs.* Reynolds number for the first truncation (exact boundary conditions). Slope of the straight line: $m = -0{\cdot}74$.

4.3 *Second truncation.*

4.3.1. *Derivation and integration of the second truncation.* The second truncation is obtained by setting $f_3 = f_3' = f_3'' = \ldots = f_4 = \ldots \equiv 0$ in (4.2*a–c*). The equations then reduce to

$$\eta f_1^{\mathrm{IV}} + 12\eta f_2'' - 4f_1''' - 24f_2' - 6\eta f_1 f_2' - \eta f_1 f_1''' + 12 f_1 f_2 + 2f_1 f_1'' + 6\eta f_1' f_2 + \eta f_1' f_1'' = 0, \tag{4.21a}$$

$$f_1^{\mathrm{IV}} + \eta^2 f_2^{\mathrm{IV}} - 4\eta f_2''' + 4f_2'' - 6f_1 f_2' - f_1 f_1''' - \eta^2 f_1 f_2''' + 2\eta f_1 f_2'' - 12\eta^2 f_2 f_2' - 3\eta^2 f_2 f_1''' + 36\eta f_2^2 + 6\eta f_2 f_1'' - 6f_1' f_2 - f_1' f_1'' + 3\eta^2 f_1' f_2'' + \eta^2 f_2' f_1'' = 0. \tag{4.21b}$$

(Equation (4.21*b*) actually results from combining (4.2*a*) and (4.2*b*) in such a way that a number of similar terms cancel.)

The boundary conditions are, at $\eta = 0$,

$$f_1(0) = f_2(0) = 0, \tag{4.22a}$$

$$f_1'(0) = f_2'(0) = 0, \tag{4.22b}$$

and, for large η, either

$$\left.\begin{aligned} f_1(\eta) &= -(\ )\eta, \\ f_2(\eta) &= -(\ )\eta^3, \end{aligned}\right\} \tag{4.22c}$$

or

$$\left.\begin{aligned} f_1(\eta) &= -\tfrac{1}{3}a\eta^{\frac{5}{3}}(\beta_0 + \beta_3 a^3\eta^2 + \ldots), \\ f_2(\eta) &= \tfrac{1}{9}\beta_0 a\eta^{-\frac{1}{3}} - \tfrac{1}{18}ab^2\beta_0^2\eta^{\frac{7}{3}} + \tfrac{4}{9}a^4\beta_3\eta^{\frac{5}{3}}, \\ &\quad -\tfrac{5}{18}a^4\beta_3\beta_0 b^2\eta^{\frac{13}{3}} + \ldots. \end{aligned}\right\} \tag{4.22d}$$

The system (4.21a, b) along with boundary conditions (4.22a–c or d) is a two-point boundary-value problem. Since the differential equations are coupled, the numerical integration must be carried out simultaneously. Again, a Runge–Kutta fifth-order scheme was employed. Similar to the first truncation, the highest derivatives f_1^{IV} and f_2^{IV} are multiplied by η and η^2, respectively, and therefore singular behaviour is present at $\eta = 0$. In order to start the numerical integration, series expansions for small η must be determined.

One finds the following series expansions, for small η, for f_1 and f_2 (Talke 1968):

$$\begin{aligned} f_1 = {} & a_2\eta^2 - \tfrac{1}{3}b_2\eta^4 - \tfrac{2}{63}a_2b_2\eta^7 + \tfrac{1}{252}a_2^3\eta^8\ln\eta + \left(\frac{167}{5.6.7.8.9.14}a_2^3 - \tfrac{1}{56}a_2b_3\right)\eta^8 \\ & - \tfrac{1}{2268}a_2^2b_2\eta^{10}\ln\eta + \frac{1}{10.9.8.7}\left(-\frac{369{,}290}{2^2.3^4.5.7}a_2^2b_2 + 10b_2b_3\right)\eta^{10} \\ & - \frac{23}{2^2.3^4.5.7.11}a_2^4\eta^{11}(\ln\eta)^2 + \left(-\frac{338{,}909}{2^4.3^6.5^2.7^2.11^2}a_2^4\right. \\ & \left. + \frac{23}{2^2.3^2.5.7.11}a_2^2b_3\right)\eta^{11}\ln\eta + a_{11}\eta^{11} + O(\eta^{12}\ln\eta) + \ldots \end{aligned} \tag{4.23a}$$

and

$$\begin{aligned} f_2 = {} & b_2\eta^2 - \tfrac{2}{9}a_2^2\eta^3\ln\eta + b_3\eta^3 - \frac{79}{2^2.5.3^5}a_2^3\eta^6 + \tfrac{1}{126}b_2^2\eta^7 - \tfrac{1}{1260}a_2^2b_2\eta^8\ln\eta \\ & + \frac{1}{7.8.10}\left(\frac{190{,}518}{2^2.3^4.5.7}a_2^2b_2 + 2b_2b_3\right)\eta^8 + \frac{23}{2^2.3^6.7}a_2^4\eta^9(\ln\eta)^2 \\ & + \left(\frac{134{,}629}{2^4.3^8.7^2.11}a_2^4 - \frac{23}{2^2.3^4.7}a_2^2b_3\right)\eta^9\ln\eta \\ & + \left(-\tfrac{55}{9}a_{11} - \frac{3979}{2^3.3^5.5.7.11}a_2^2b_3 + \frac{146{,}330{,}391}{2^5.3^{10}.5^2.7^2.11^2}a_2^4\right)\eta^9 + O(\eta^{10}\ln\eta) + \ldots. \end{aligned} \tag{4.23b}$$

We note that four free constants (a_2, b_2, b_3, a_{11}) occur in the series expansions. These constants are to be determined from the integral curves which satisfy the

asymptotic boundary conditions (4.22*c* or *d*). The numerical integration can now be carried out by assigning particular values to the four undetermined constants.

To find the dependence of the integral curves on the four constants, the parameters a_2, b_2 and b_3 were fixed arbitrarily, and the integration was performed for different values of a_{11}. For the same values of a_{11}, but different values of b_3, the integration was carried out again, a_2 and b_2 still being fixed as before. Thereafter, the value of b_2 was changed, and every time the above procedure repeated. Finally, the integral curves were obtained as functions of the four parameters by assigning different values to a_2 and repeating in succession the steps indicated above.

4.3.2. *Simplified boundary conditions.* In this section the solution of the second truncation (4.21*a*, *b*), subject to the simplified boundary conditions (4.22*c*), will be given. The differential equations are satisfied for large η by

$$f_1 \sim -k_1\eta, \tag{4.24a}$$

$$f_2 \sim -k_2\eta^3. \tag{4.24b}$$

Thus solutions satisfying the simplified boundary conditions exist and can be obtained by the following iteration process: If a_2, b_2 and b_3 are fixed arbitrarily, and a_{11} is varied, one finds that for large negative values of a_{11} the curves of f_2^{IV} increase to plus infinity, whereas for small positive values of a_{11} the curves go to minus infinity. By iteration the value of a_{11} can be determined so that f_2^{IV} remains zero or grows slowly for large η. For this a_{11} the second asymptotic boundary condition $f_2 \sim -k_2\eta^3$ is thus satisfied. Examining the curves f_1'' and f_1^{IV} for the above a_{11}, one finds that both curves go to plus infinity if b_3 is large and positive, whereas they go to minus infinity if b_3 is large and negative. Therefore, a value of b_3 must exist for which f_1'' and f_1^{IV} become zero or stay small for large η. This value of b_3 can be determined by trial, using the arithmetic mean-value technique of § 4.2.2. The integral curves obtained in this way satisfy the asymptotic boundary conditions. At this stage of the solution the two constants, a_2 and b_2 are still arbitrary. However, from the first truncation it is known that the solution must be sought in a certain range of a_2 values. Thus, the constant a_2 can be chosen arbitrarily, and therefore only b_2 is left unknown. This last constant is obtained by considering the numerical matching condition of § 4.2.2, which requires that

$$f_1(\eta) = -c_0\eta|_{\eta=\eta_{\mathrm{M}}}, \tag{4.25a}$$

$$f_2(\eta) = -c_2\frac{\eta^3}{12R}\bigg|_{\eta=\eta_{\mathrm{M}}}. \tag{4.25b}$$

Again, the value of η_{M} is found from the requirements that the value and the axial distribution of the centreline velocity equal those of Goldstein's solution in the matching region. As with the first truncation, the Reynolds number associated with a_2 is found by matching f_1, but a second Reynolds number is found from (4.25*b*). In general, both Reynolds numbers are not equal and therefore the procedure described above must be repeated for different values of b_2 until agreement of both Reynolds numbers is obtained.

In figure 10 the solution curves are presented for a fixed value of a_2. One observes that the solution curves f_1 of the second truncation are very similar to the solution curves of the first truncation, if the same value of a_2 is considered. Furthermore, it is found that a variation of b_2 resulting in a change of an order of magnitude of f_2 affects the solution curve for f_1 by only a small amount. As in

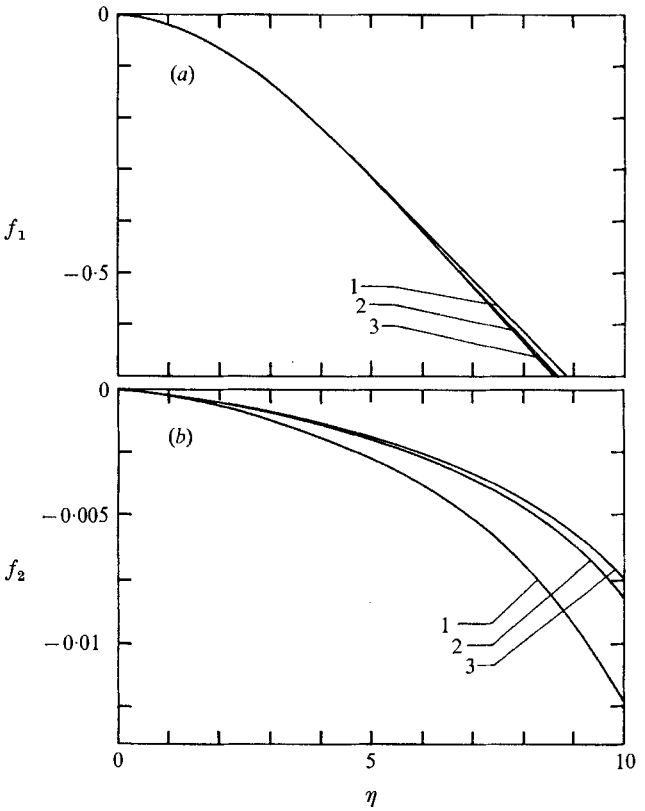

FIGURE 10. Solution curves for the second truncation (simplified boundary conditions):

	(*a*)		(*b*)
	$a_2 = -0{\cdot}015$		$a_2 = -0{\cdot}015$
1	$b_2 = -0{\cdot}00035$	1	$b_2 = -0{\cdot}00035$
2	$b_2 = -0{\cdot}000327$	2	$b_2 = -0{\cdot}000327$
3	$b_2 = -0{\cdot}0003225$	3	$b_2 = -0{\cdot}0003225$

the first truncation, a one-to-one correspondence between solution curve and Reynolds number is established. A comparison of the results of the first and second truncations shows that the Reynolds numbers associated with a certain value of a_2 are approximately 35 % higher for the second truncation.

4.3.3. *Exact boundary conditions.* We shall now take up the solution of the differential equations (4.21 *a*, *b*) subject to the exact boundary conditions. The considerations of §4.2.3 regarding the existence of a solution are still appropriate, i.e. η must be sufficiently small so as to ensure a bounded solution, but at

the same time it must be large enough so as to allow 'asymptotic' behaviour. With these assumptions the appropriate boundary conditions are

$$f_1 = -\tfrac{1}{3}a\beta_0\eta^{\frac{5}{3}} \tag{4.26a}$$

and

$$f_2 = \tfrac{1}{9}\beta_0 a\eta^{-\frac{1}{3}} - \tfrac{1}{18}ab^2\beta_0^2\eta^{\frac{7}{3}}. \tag{4.26b}$$

Substitution of (3.25) and (3.26), and rearrangement, leads to

$$R = \left[-\tfrac{1}{6}\beta_0 \frac{1}{f_1/\eta^{\frac{5}{3}}}\right]^3 \tag{4.27a}$$

and

$$R = \tfrac{1}{18}\beta_0\left[\frac{1}{\dfrac{-f_2}{\eta^{\frac{7}{3}}} + \tfrac{1}{18}\beta_0 \dfrac{1}{R^{\frac{1}{3}}\eta^{\frac{8}{3}}}}\right]^{\frac{3}{2}}. \tag{4.27b}$$

The solution for the second truncation satisfying (4.26a, b) or (4.27a, b) is found by an iteration process. Because of the apparent similarities to §4.3.2, only the main steps of the analysis will be presented.

With a_2, b_2 and b_3 fixed, an integral curve proportional to $\eta^{\frac{5}{3}}$ can be obtained by iteration on a_{11}. The iteration is repeated for different choices of b_3, thus determining the value of b_3 that satisfies (4.27b). Two Reynolds numbers, one from (4.27a) and one from (4.27b), are found in this way, and unless they are equal the above calculations are repeated for a different value of b_2. The set of constants b_2, b_3 and a_{11}, which makes both Reynolds numbers identical, is the correct set of initial conditions, and determines the unique Reynolds number associated with a_2.

The solution curves satisfying (4.26a, b) are shown in figure 11 for a fixed value of a_2. It can be seen that the solution curves for f_1 of the second truncation are similar to the solution curves f_1 of the first truncation for the same value of a_2. The Reynolds numbers of the second truncation are approximately 25 % higher than the ones calculated from the first truncation in §4.2.3.

4.3.4. *Distribution of skin friction and region of influence.* The distribution of the coefficient of skin friction is now obtained from

$$\tfrac{1}{2}c_f = -\left[\frac{f_1''(0)}{(2(x_1/L)R)^{\frac{1}{2}}} + f_2''(0)\,(2(x_1/L)R)^{\frac{1}{2}}\right]. \tag{4.28}$$

As in the first truncation, the skin friction becomes infinite at the trailing edge. If $\frac{1}{2}c_f$ is calculated from (4.28) no numerical matching with the Blasius value is found to occur; of the two sets of solutions, the curves calculated from the results of the exact boundary conditions approach the Blasius value closer than those based on the simplified boundary conditions (cf. figure 12). Both curves of $\frac{1}{2}c_f$ have in common that a clearly defined minimum exists, at the distance

$$\frac{x_1}{L} = \frac{f_1''(0)}{2f_2''(0)\,R}; \tag{4.29}$$

we assume that the region of influence is given by (4.29). Thus, a correspondence between Reynolds numbers and region of influence is obtained. The plot of

$\ln(x_{1R}/L)$ *vs.* $\ln R$ shows all points to lie on a straight line with a slope $m = -0{\cdot}752$ (simplified boundary conditions, cf. figure 13) and $m = -0{\cdot}759$ (exact boundary conditions, cf. figure 14). Therefore, the functional relationship $(x_1/L) = (x_1/L)(R)$ is given by

$$x_1/L \sim R^{-0{\cdot}752} \quad \text{(simplified boundary conditions)}, \tag{4.30a}$$

and

$$x_1/L \sim R^{-0{\cdot}759} \quad \text{(exact boundary conditions)}. \tag{4.30b}$$

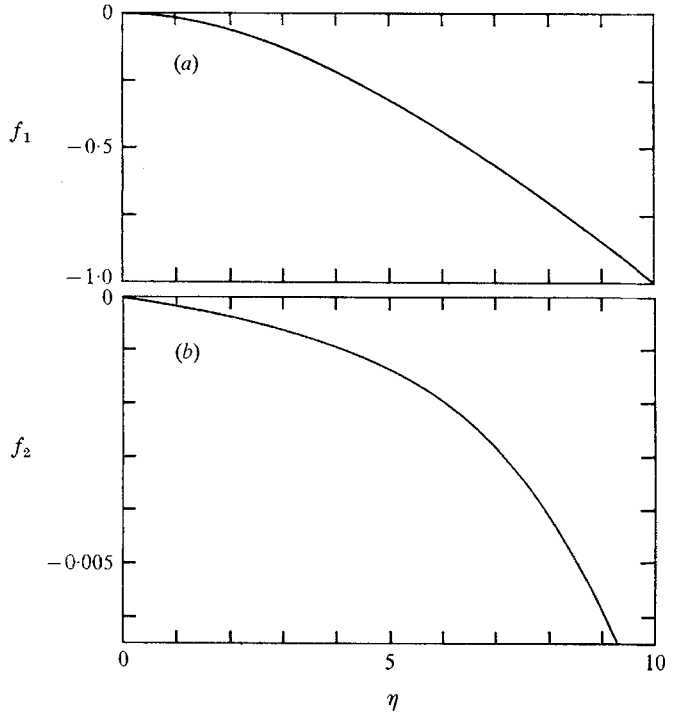

FIGURE 11. Solution curves for the second truncation (exact boundary conditions):

(*a*)	(*b*)
$a_2 = -0{\cdot}015$	$a_2 = -0{\cdot}015$
$b_2 = -0{\cdot}000261$	$b_2 = -0{\cdot}000261$

From (4.30*a*, *b*) it follows that the results of the second truncation, with respect to the functional dependence $(x_1/L) = (x_1/L)(R)$, are in excellent agreement with the theoretical predictions. There is, however, no numerical matching obtained with the shear stress distribution of the Blasius solution. Yet, since only two terms are calculated in the series expansion, a third truncation might possibly lie between the first and second, and thus give an even better numerical approach to the Blasius solution.

5. Discussion and conclusions

By application of the method of series truncation to the full Navier–Stokes equations, the flow near the trailing edge of a flat plate has been analyzed.

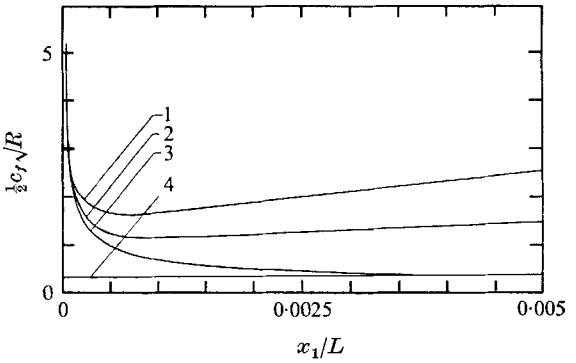

FIGURE 12. Distribution of skin friction at the trailing edge:
1 Second truncation, simplified boundary condition ($a_2 = -0{\cdot}015$).
2 Second truncation, exact boundary conditions ($a_2 = -0{\cdot}015$).
3 First truncation ($a_2 = -0{\cdot}015$).
4 Blasius solution.

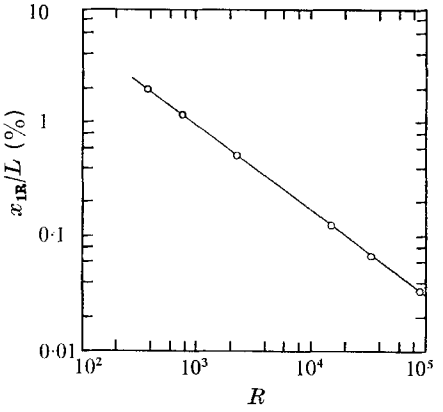

FIGURE 13. Region of influence *vs.* Reynolds number for the second truncation (simplified boundary conditions). Slope of the straight line: $m = -0{\cdot}752$.

Solutions have been obtained for the first and second truncations, for both simplified and exact boundary conditions. The results were seen to be similar for both sets of boundary conditions.

The functional dependence of the region of influence on the Reynolds number was found to be given by $x_1/L \sim R^m$, where m was determined as:

$m = -0{\cdot}747$ (first truncation, simplified boundary conditions),

$m = -0{\cdot}74$ (first truncation, exact boundary conditions),

$m = -0{\cdot}752$ (second truncation, simplified boundary conditions),

$m = -0{\cdot}759$ (second truncation, exact boundary conditions).

Order of magnitude arguments (§3.1) indicate that we should expect $m = -0{\cdot}75$. Thus, the series truncation solution gives as the domain of influence of the trailing edge, results which are in remarkable agreement with the theoretical

prediction. The significance of this agreement lies in the fact that, as far as the authors are aware, this is the only analysis, either analytic or numerical, which yields the region of influence proportional to $R^{-0.75}$, without any *à priori* assumption about its magnitude. Stewartson (1968), in his analysis of this problem, at the outset assumed the trailing edge region to be of this size, and stretched his variables accordingly. It is worth emphasizing again, then, that in solving the full Navier–Stokes equations near the trailing edge there has been no explicit or implicit assumption about the extent of the trailing edge region, the series truncation solution itself determining its size.

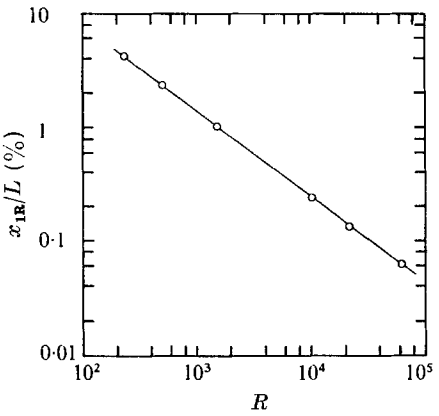

FIGURE 14. Region of influence *vs.* Reynolds number for the second truncation (exact boundary conditions). Slope of the straight line: $m = -0{\cdot}759$.

The skin friction, as calculated from the first and second truncations, was found to be singular at the trailing edge. Furthermore, throughout the trailing edge region c_f turns out to be larger than the Blasius value. Therefore, an additional drag acts on the plate due to the trailing edge. Since the trailing edge region is of $O(R^{-\frac{3}{4}})$, the trailing edge correction will contribute to the integrated drag coefficient a term of $O(R^{-\frac{5}{4}})$.

Qualitatively, the results of the first truncation for the distribution of skin friction are in very good agreement with Dennis & Dunwoody's (1966) numerical calculations. However, due to the small scale of Dennis & Dunwoody's solution curves a detailed quantitative comparison with the present results is not possible. Using a somewhat different method, based much more on finite-differences than the original work of Dennis & Dunwoody, Dennis & Chang (1969, personal communication) have obtained improved results for the flat plate. However, due to high accuracy standards and the resultant small grid size, solutions have been obtained only for Reynolds numbers up to 200. In figure 15 the predictions of Dennis & Chang and the present theory for the variation of skin friction near the trailing edge are compared for the closest corresponding Reynolds numbers for which results are available. Since the second truncation solution does not numerically patch on to the Blasius solution as one moves upstream, only the results for the first truncation are shown in the figure. The agreement between the

first truncation solution and the finite-difference solution of Dennis & Chang is seen to be quite good even at the low Reynolds numbers, for which the theory is weakest. Because the second truncation does not numerically match with the Blasius value, no further information with respect to the distribution of the shear stress can be obtained. Although a numerical solution of the third truncation might be useful in this matter, limitations on the available computer facilities made this impossible at the present time.

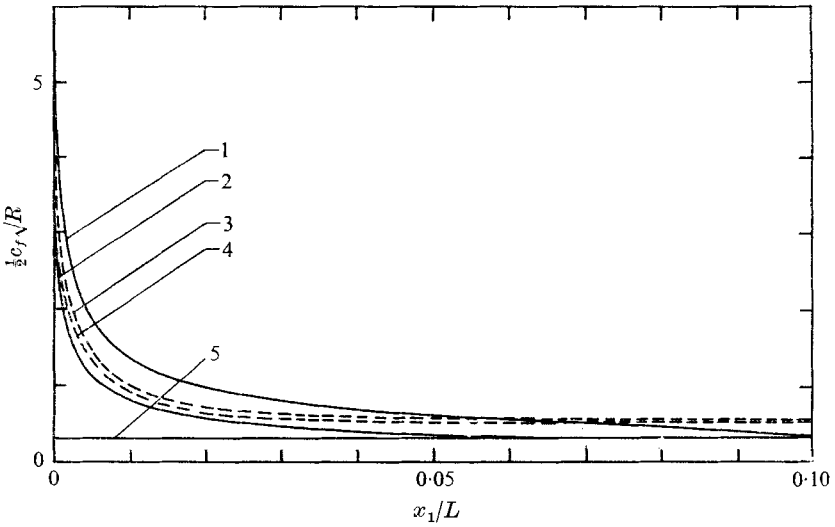

FIGURE 15. Distribution of skin friction at the trailing edge. ——, first series truncation with exact boundary conditions; – – –, Dennis & Chang 1969:

1 $R = 106$ 4 $R = 200$
2 $R = 411$ 5 Blasius solution
3 $R = 100$

After the completion of the work described in this paper, a finite-difference solution (Plotkin & Flügge-Lotz 1968), completed at the same time, came to the attention of the authors. Plotkin & Flügge-Lotz non-dimensionalize the governing Navier–Stokes equations in the same way as for a boundary layer, but retain the terms involving Reynolds number in the denominator, terms which are discarded in the usual boundary layer equations. With the assumption that $|p_x| \gg |p_y|$, the pressure at any x is taken as the average of the values in the free-stream and at the wall, the latter calculated from the y momentum equation. For this p_x, the continuity equation and x momentum equation can then be solved for u and v. The equations are solved by finite-differences, for Reynolds numbers larger than 10^5, in a rectangular region about the trailing edge. The Blasius solution is imposed as the boundary condition at the upstream face. With this formulation, Plotkin & Flügge-Lotz find that the region of influence of the trailing edge is much larger than $O(R^{-\frac{3}{4}})$. In fact, both the Navier–Stokes region of $O(R^{-\frac{3}{4}})$ and the inviscid region of $O(R^{-\frac{1}{2}})$, described in § 3.1, are smaller than the mesh size in their numerical solution. For example, for $R = 10^5$, they

find the influence of the trailing edge extends a distance $0{\cdot}05L$, whereas $R^{-\frac{3}{4}}L \approx 0{\cdot}00018L, R^{-\frac{1}{2}}L \approx 0{\cdot}00316L$; the streamwise mesh size for this computation was $\Delta x = 0{\cdot}006$. It is not clear how this very large domain of influence comes about. The only mechanism responsible for upstream influence in the formulation of Plotkin & Flügge-Lotz is upstream diffusion, due to the u_{xx}/R term in the x momentum equation. But, as noted by the authors, since $R \geqslant 10^5$ in all the calculations, this term is practically of negligible magnitude compared to the other terms, and in particular compared to the lateral diffusion term. Yet, inexplicably, this term causes significant diffusion to a distance three times the boundary-layer thickness. (As will be discussed in the next paragraph, the displacement effect of the boundary layer on the outer inviscid flow has recently been put forth as a mechanism that can lead to a large region of influence. This effect, however, is neglected in the Plotkin & Flügge-Lotz analysis, and therefore cannot be responsible for this effect in their work.) The root of the paradox may lie in the non-dimensionalization and the numerical scheme used. This latter possibility is suggested by the fact that the numerical solution is strongly dependent on the mesh size. It should also be pointed out that solutions could not be obtained for Reynolds numbers appreciably smaller than 10^5 (or for mesh sizes $\Delta x < 0{\cdot}0015L$). Also, because of the existence of the singularity at the trailing edge, a solution can only be obtained outside the immediate neighbourhood of the trailing edge. It would be impossible to use the present formulation of Plotkin & Flügge-Lotz to consider the $O(R^{-\frac{3}{4}})$ Navier–Stokes region, because in this region the assumptions $|p_y| \ll |p_x|$ and weak upstream influence would be violated.

In addition to the numerical solution discussed above, the authors recently became aware, after completion of this work, of new theoretical studies of the trailing edge problem by Stewartson (1969) and Messiter (1969).† These analyses are very similar. Their authors claim that, although a Navier–Stokes region of size $O(R^{-\frac{3}{4}})$ still exists, the boundary layer on the plate is already modified at a distance $O(R^{-\frac{3}{8}})$ from the trailing edge; that is, a distance much greater than the $O(R^{-\frac{3}{4}})$ found here. This estimate results from taking into account the induced pressure gradient due to the displacement effect of the boundary layer on the outer flow. (The order estimate $R^{-\frac{3}{8}}$ is the same as that given by Lighthill (1953) for the upstream influence of a small disturbance in a supersonic boundary layer.) The intermediate region of $O(R^{-\frac{3}{8}})$, for consistency, must itself be subdivided into three mutually dependent subregions or 'decks', each of the same streamwise dimension $O(R^{-\frac{3}{8}})$, but with thicknesses normal to the plate of $O(R^{-\frac{3}{4}})$, $O(R^{-\frac{1}{2}})$ and $O(R^{-\frac{3}{8}})$, respectively. Stewartson and Messiter develop the equations appropriate for each of these subregions and the necessary conditions to match them together. (Stewartson also demonstrates that his earlier Oseen solution (1968) for the central Navier–Stokes region of $O(R^{-\frac{3}{4}})$ is still valid, and can be matched to the triple deck provided that the Blasius skin friction value, used in the uniform-shear upstream boundary condition, is replaced by the actual skin friction predicted by the triple deck.) It is difficult

† The authors thank one of the referees for having brought these papers to their attention prior to publication.

to reconcile the size of the domain of influence $O(R^{-\frac{3}{8}})$, claimed by these authors, with the $O(R^{-\frac{1}{4}})$ found in the present analysis. It might perhaps be simply reiterated that in the solution obtained here, no *à priori* estimate of the domain was made, the basic assumption being that the Navier–Stokes solution must at *some* point pass over into the Goldstein solution. Thus any fine structure, such as presented by Stewartson and Messiter, should be implicitly contained in the present results, and as we have seen these results indicate, with remarkable precision, that the region of influence of the trailing edge extends upstream only a distance of $O(R^{-\frac{1}{4}})$.

This work was supported by the Office of Naval Research, Mechanics Branch (Contract Nonr-222(45)).

REFERENCES

Blasius, H. 1908 Grenzschichten in Flüssigkeiten mit kleiner Reibung. *Z. Math. Phys.* **56**, 1.

Burgers, J. M. 1924 The motion of a fluid in the boundary layer along a plane smooth surface. *Proc. 1st Int. Congr. Appl. Mech.* Delft.

Cheng, R. T. 1967 An investigation of the laminar flow around the trailing edge of a flat plate. *Univ. Calif., Berkeley, Aero. Sci. Rept.* AS-67-8.

Davis, R. T. 1967 Laminar incompressible flow past a semi-infinite flat plate. *J. Fluid Mech.* **27**, 691.

Dennis, S. C. R. & Dunwoody, J. 1966 The steady flow of a viscous fluid past a flat plate. *J. Fluid Mech.* **24**, 577–595.

Goldburg, A. & Cheng, S. I. 1961 The anomaly in the application of PLK and parabolic co-ordinates to the trailing edge boundary layer. *J. Math. Mech.* **10**, 529.

Goldstein, S. 1930 Concerning some solutions of the boundary layer equations in hydrodynamics. *Proc. Camb. Phil. Soc.* **26**, 1.

Goldstein, S. 1933 On the two-dimensional steady flow of a viscous fluid behind a solid body. *Proc. Roy. Soc. Lond.* A **142**, 545–573.

Grove, A. S., Petersen, E. E. & Acrivos, A. 1964 Velocity distribution in the laminar wake of a parallel flat plate. *Phys. Fluids*, **7**, 1071.

Hansen, M. 1930 Velocity distribution in the boundary layer of a submerged plate. *NACA*, Tech. Memo. 585.

Imai, I. 1964 On the viscous flow near the trailing edge of a flat plate. *Proc. 11th Int. Congr. appl. Mech.*, Munich.

Kuo, Y. H. 1953 On the flow of an incompressible viscous fluid past a flat plate at moderate Reynolds numbers. *J. Math. Phys.* **32**, 83.

Lighthill, M. J. 1953 On boundary layers and upstream influence. I. A comparison between subsonic and supersonic flows. *Proc. Roy. Soc. Lond.* A **217**, 478.

Messiter, A. F. 1969 Boundary-layer flow near the trailing edge of a flat plate. *SIAM J. appl. Math.* (To be published.)

Nikuradse, J. 1942 Laminare Reibungsschichten an der längsangeströmten Platte. *Zentrale für wiss. Berichtswesen*, Berlin.

Plotkin, A. & Flügge-Lotz, I. 1968 A numerical solution for the laminar wake behind a finite flat plate. *Trans. ASME* (Ser. E), *J. appl. Mech.* **35**, 625.

Stewartson, K. 1968 On the flow near the trailing edge of a flat plate. *Proc. Roy. Soc. Lond.* A **306**, 275.

Stewartson, K. 1969 On the flow near the trailing edge of a flat plate. II. *Mathematika*, **16**, 106.

Talke, F. E. 1968 An analysis of the flow near the trailing edge of a flat plate using series truncation. *Univ. Calif., Berkeley, Aero Sci. Rept.* AS-68-11.

Van Dyke, M. 1964*a* *Perturbation Methods in Fluid Mechanics*. New York: Academic.

VAN DYKE, M. 1964*b* The circle at low Reynolds number as a test of the method of series truncation. *Proc. 11th Int. Congr. appl. Mech.*, Munich.

VAN DYKE, M. 1965 A method of series truncation applied to some problems in fluid mechanics. *SUDAER* no. 247, *Dept. of Aeronautics and Astronautics, Stanford Univ.*

VAN DYKE, M. 1967 A survey of higher-order boundary layer theory. *SUDAER* no. 326, *Dept. of Aeronautics and Astronautics, Stanford Univ.*